J Solid State Eletrochem (2004) 8: 252–259
DOI 10.1007/s10008-003-0439-z

ORIGINAL PAPER

T. Grygar · T. Rojka · P. Bezdička
E. Večerníková · F. Kovanda

Voltammetric and X-ray diffraction analysis of the early stages of the thermal crystallization of mixed Cu,Mn oxides

Received: 27 April 2003 / Accepted: 3 July 2003 / Published online: 27 September 2003

Abstract Mixed Cu,Mn, Cu,Mn,Al, Cu,Mg,Mn, and Cu,Mg,Mn,Al oxides were obtained by calcination of amorphous basic carbonate (Cu,Mn oxides) or hydrotalcite-like precursors at 300–800 °C. The product composition was characterized by chemical analysis, XRD, and voltammetry of the microparticles. The XRD amorphous portion was detected indirectly by XRD and directly by voltammetry. Tenorite (CuO) and spinels were the main crystalline components of the oxide mixtures. The presence of Al shifted the onset of the crystallization of XRD-detectable tenorite and spinel to temperatures higher by 100–200 °C, and the presence of Mg shifted tenorite crystallization by 100 °C, but voltammetry was able to detect these phases even in XRD-amorphous or nanocrystalline calcines. Voltammetry is hence suitable for analysis of poorly crystalline oxides that can be used in heterogeneous catalysis.

Keywords Amorphous phases · Cu,Mn oxides · Hydrotalcite · Microparticles · Voltammetry

Introduction

According to widely accepted practical experience, for a transition metal oxide to be a good catalyst it should have a small particle size, poor crystallinity, and/or a defect structure. Such materials are poorly characterized by XRD: a specimen with a specific surface area of 150 m^2/g can be composed of particles with a characteristic size of ~10 nm that is not very much above the coherence length required to obtain a well-resolved diffraction pattern. Other methods are hence required to characterize such a poorly ordered solid if the catalyst's functionality is to be understood and optimized. EXAFS [1, 2, 3] and XPS [4, 5] are frequently used for this task, but they are not well suited to more complex oxide mixtures. Redox catalysts are frequently based on electrochemically active transition metal oxides, and hence electroanalytical techniques are worth testing for the task. Several electroanalytical studies have recently dealt with transition-metal-containing catalysts, such as Fe zeolites [6] and Ni,Mn oxides [7]. In Fe zeolites [6], voltammetry was found suitable for the complete speciation of Fe(III) species present in the catalyst. In the case of Ni,Mn oxides [7], voltammetry directly detected XRD-amorphous matter rich in Mn^{IV} that was present at a calcination temperature of ~300 °C. In principle, voltammetry can have a similar nature as temperature-programmed reduction (TPR): both techniques are based on analysis via heterogeneous reaction kinetics. In Cu-containing oxides, TPR can distinguish nanocrystalline and bulk CuO [8] on the basis of their different reactivities. The Mn valence in non-stoichiometric Ni,Mn spinel was estimated by TPR from hydrogen consumption [9]. Both Mn oxides and CuO can also be studied by voltammetry, employing reductive dissolution and reduction to metal, respectively.

Cu,Mn-containing metal oxides can be easily obtained by calcination of mixed carbonates [1], metal nitrates [5], or hydrotalcite-like compounds. Cu,Mn oxides have recently been tested in the combustion of CO [1], NH_3 [5], and organic pollutants. Amorphous copper manganite, $CuMn_2O_4$ ("hopcalite"), is probably the best-known catalyst of this type used in the combustion of volatile organic compounds. In the present work, Cu,Mn-containing oxide mixtures were prepared by thermal decomposition of hydrotalcite-like precursors or hydroxycarbonates and characterized by chemical analysis, XRD, and voltammetry. The aim was to characterize the phase composition of the Cu- and Mn-containing mixed oxides obtained by the thermal treat-

T. Grygar (✉) · P. Bezdička · E. Večerníková
Institute of Inorganic Chemistry, AS CR,
250 68 Řež, Czech Republic
E-mail: grygar@iic.cas.cz

T. Rojka · F. Kovanda
Department of Solid State Chemistry, Institute of Chemical Technology, Technická 5, 166 28 Prague, Czech Republic

ment of the above-mentioned precursors at temperatures of 300–800 °C. Calcines obtained at lower temperatures (300–500 °C) are almost XRD amorphous but actually such solids could be interesting for their application in heterogeneous catalysis. Voltammetry was used to compare the low-temperature calcines with those obtained at temperatures up to 800 °C that were conveniently and unequivocally analyzed by powder XRD.

Experimental

Samples of Cu^{II}-Mn^{III} hydroxycarbonate with a Cu:Mn molar ratio of 4:2 (denoted as Cu4Mn2) and Cu^{II}-Mg^{II}-Mn^{III}-Al^{III} hydrotalcite-like compounds with Cu:Mg:Mn:Al molar ratios of 2:2:2:0, 4:0:1:1, and 2:2:1:1 (denoted as Cu2Mg2Mn2, Cu4MnAl, and Cu2Mg2MnAl, respectively) were prepared by coprecipitation. A series Mg4Mn2 was also prepared as a reference without Cu. An aqueous solution (450 mL) containing appropriate amounts of metal nitrates, $Cu(NO_3)_2.3H_2O$, $Mg(NO_3)_2.6H_2O$, $Mn(NO_3)_2.4H_2O$, and/or $Al(NO_3)_3.9H_2O$, with a M^{II}/M^{III} molar ratio of 2 and a total metal ion concentration of 1.0 M was added dropwise with vigorous stirring to 200 mL of 0.5 M Na_2CO_3 solution. The addition took about 1 h. During the synthesis the temperature was maintained at 25 °C and the pH at about 10 by simultaneous addition of a 3 M NaOH solution. The resulting suspension was then maintained for 18 h at 25 °C with stirring. The product was filtered off and washed repeatedly with distilled water and dried overnight at 60 °C in air. The dried precursors were calcined at chosen temperatures in the range 300–800 °C in air for 2 h. The elemental composition was checked by flame AAS (Cu, Mg, Mn) and chelatometric titration (Al). Analysis of the mean Mn valence was performed after dissolution of calcines in a solution of KI acidified by HCl by titration of the evolved I_2 by $Na_2S_2O_3$. The mean Mn valence was calculated assuming that Cu and Mg are divalent and Al trivalent. Malachite [$Cu_2CO_3(OH)_2$] and tenorite (CuO) reference samples were prepared by precipitation of $CuCl_2$ solutions by additions of Na_2CO_3 at room temperature and NaOH at 90 °C, respectively.

Decomposition of the precursors was studied by thermal analysis (TG/DTA) using a Netzsch STA 409 instrument equipped with a quadrupole mass spectrometer (QMS 403/4, Balzers) for analysis of the gases evolved during sample heating. The heating rate of 10 °C/min in air with a flow rate of 75 mL/min and 50 mg of sample were used. Gaseous products were continually monitored for the chosen mass numbers $m/z = 18$ (H_2O^+) and 44 (CO_2^+).

Powder XRD patterns were recorded using a Seifert XRD 3000P instrument with Co Kα radiation ($\lambda = 0.179$ nm, graphite monochromator, goniometer with Bragg-Brentano geometry) in the 2θ range 12–75° with a step size of 0.05°. XRD patterns were processed by PowderCell 2.4 (Kraus and Nolze, Federal Institute for Materials Research and Testing, Berlin, Germany) and DiffracPlus Topas, release 2000 (Bruker AXS, Germany). The structural models were taken from Inorganic Crystal Structure Database, ICSD/retrieve 2.01 [10]. Both programs perform full-profile fitting by refining lattice parameters and profile functions. DiffracPlus Topas also provides estimates of particle sizes (mean coherence lengths) from the diffraction line broadening. Neither specific line broadening nor systematic deviation of certain diffraction line intensities was observed, and hence the fitting did not include microstrain or preferential orientation. Integral intensities of selected lines were calculated by OriginPro7.0 using the direct integration fit without any data smoothing or fitting to a mathematical function. The comparison of integral intensities was possible owing to the constant geometry of the diffraction experiment and a sufficiently (''infinitesimally'') thick layer of the samples.

Voltammetry of microparticles (VMP) was performed with a paraffin-impregnated graphite working electrode, a Pt-plate counter electrode, and a saturated calomel reference electrode, using potentiostat μAutolab (EcoChemie, the Netherlands) [12, 13]. A CH_3CO_2H/CH_3CO_2Na buffer was used as the supporting electrolyte with 0.2 M total concentration of acetate ions and pH 4.7. To evaluate the influence of pH, 0.2 M CH_3CO_2H (pH 2.4) and buffers with a CH_3CO_2H/CH_3CO_2Na ratio of 4:1, 1:4, and 1:9 and pH values of 3.9, 5.3, and 5.7, respectively, were used. Cyclic voltammetry with a scan rate of 3 mV/s was sufficient to convert at least 95% of the sample deposit on the working electrode in the first scan. Scanning was started from an open-circuit potential cathodically and cycled between −0.9 and +0.8 V vs. SCE that ensured both reduction of $Mn^{III,IV}$ and Cu^{II} in a cathodic scan and reoxidation of Cu^0 in an anodic scan. Because the software provided with the potentiostat cannot be used to separate the charges of overlapping peaks, the peak-fitting module of OriginPro7.0 was used for that purpose. The shapes of the voltammetric peaks of irreversibly reacting powders must involve at least three parameters: the rate coefficient at a given potential controlling the peak-potential, a formal charge-transfer coefficient controlling the peak potential and (mainly) the shape of the ascending part of the peak, and a heterogeneity parameter controlling (mainly) the shape of the descending part of the peak. The heterogeneity parameter changes with the actual potential following, which complicates the design of an optimal ''correct'' peak-fitting function. An empirically chosen function that seemed to be most suitable for the asymmetric voltammetric peaks of solid reactants from the set of functions provided by the Origin peak-fitting module was a function denoted as ''Asym2sig'':

$$I = \frac{A}{1+\exp[-(E-E_P+w_{1/2})/w_2]}\left(1-\frac{1}{1+\exp[-(E-E_P-w_{1/2})/w_3]}\right) \quad (1)$$

Results

Sample characterization

The ratios of the metal constituents in the series studied are listed in Table 1. Except for the XRD-amorphous Cu4Mn2 precursor, all other precursors had a hydrotalcite-like structure according to XRD. Under the dynamic conditions of the TG measurement, the main portion of CO_2 and H_2O was evolved below 400 °C with DTG maxima between 140 and 270 °C, which agrees with the decomposition temperature of hydrotalcites of transition metals [4, 8, 9, 14]. A minor portion of CO_2 (2–4 wt% of the precursor weight) escaped at an even higher temperature: 480 °C (Cu4Mn2), 560 °C (Cu2Mg2Mn2), 540 °C (Cu4MnAl), and 600 °C (Cu2Mg2MnAl). Similar retention of a certain fraction of carbonates in Cu-hydrotalcite-like compounds has been described [14], but it was not observed at calcination of Cu-free hydrotalcite-like compounds, including the precursor Mg4Mn2. The nature of the process is not known.

The formal valence of Mn reached its maximal value in calcines obtained at 300–500 °C (Table 1), while in the precursors it was 2.0 (Cu4Mn2), 3.3 (Cu4MnAl), and 3.2 (Cu2Mg2MnAl). Pure Mn oxides are not oxidized by air to Mn^{IV} unless Mn^{III} ions are present in an appropriate structure, such as spinel. Mg presence in the samples obviously caused the growth of the mean Mn valence with respect to Mg-free samples.

Table 1 Elemental composition of the precursors and Mn valence in calcines, calculated from chemical analyses

Notation	Elemental composition	Mn formal valence					
		300 °C	400 °C	500 °C	600 °C	700 °C	800 °C
Cu4Mn2	Cu:Mn 2.02:1.00	3.25	3.25	3.37	3.33	3.25	3.08
Cu2Mg2Mn2	Cu:Mg:Mn 1.02:0.85:1.00	3.70	3.74	3.70	3.71	3.61	3.62
Cu4MnAl	Cu:Mn:Al 3.98:1.00:0.98	3.89	3.87	3.45	3.12	2.89	3.16
Cu2Mg2MnAl	Cu:Mg:Mn:Al 1.96:1.84:1.00:1.03	3.95	4.02	3.72	3.63	3.60	3.71

Table 2 The results of XRD data processing of Cu4Mn2 calcines. *D* denotes crystallite size obtained from XRD line broadening; *a* is the spinel lattice parameter. All crystalline species are included

Parameter	300 °C	400 °C	500 °C	600 °C	700 °C	800 °C
Tenorite content (%)[a]	–	39	39	39	42	47
Tenorite integral intensity (arbitrary units)[b]	56	158	218	240	293	300
Tenorite*D* (nm)	6	20	23	36	85	78
Spinel integral intensity (arbitrary units)[c]	0	38	52	67	64	52
Spinel*a* (Å)	–	8.281(2)	8.295(1)	8.294(2)	8.316(0)	8.320(1)
Spinel*D* (nm)	–	10	23	60	98	44
Spinel formula	–	$Cu_{1.35}Mn_{1.63}O_4$	$Cu_{1.32}Mn_{1.59}O_4$	$Cu_{1.37}Mn_{1.58}O_4$	$Cu_{1.24}Mn_{1.70}O_4$	$Cu_{1.18}Mn_{1.82}O_4$
R_{WP}	–	23.1	21.3	21.5	27.8	27.3

[a]Percentage in crystalline fraction
[b]Sum of diffraction lines (200) and (111)
[c]Diffraction line (400)

Table 3 The results of XRD data processing of Cu2Mg2Mn2 calcines. Abbreviations as in Table 2. Nanocrystalline spinel and periclase ($a \approx 4.17$ Å) are present in 300 °C calcine. All crystalline species are included. Approximate spinel formula is $Cu_{0.7}Mg_{1.0}Mn_{1.2}O_4$

Parameter	400 °C	500 °C	600 °C	700 °C	800 °C
Murdochite content (%)[a]	32	7	0	0	0
Tenorite content (%)[a]	7	17	17	19	20
Tenorite integral intensity (arbitrary units)[b]	14	87	127	165	169
Tenorite*D* (nm)	11	15	27	55	86
Spinel integral intensity (arbitrary units)[c]	–[d]	96	91	104	107
Spinel*a* (Å)	8.27(1)	8.312(2)	8.324(0)	8.317(0)	8.324(0)
Spinel*D* (nm)	< 3	7	19	64	121
R_{WP}	–	18.4	21.3	18.5	21.5

[a]Percentage in crystalline fraction
[b]Sum of diffraction lines (200) and (111)
[c]Diffraction line (400)
[d]Overlap with the periclase diffraction

XRD phase analysis

The phase composition was evaluated by comparison of the diffractograms with the PDF database [11] to identify the phases present, and then by full-profile analysis using models adopted from the ICSD database [10]. The results obtained by XRD of Al-free samples are summarized in Tables 2 and 3, and Al-containing samples in Tables 4 and 5. The crystalline components of the oxide mixtures were tenorite (CuO), spinel ($M_{3-x}O_4$), and the cubic phase Mg_6MnO_8, isostructural with murdochite. The murdochite structure is derived from rock salt by substituting 1/4 of the cations by pairs [Mn^{IV} + cationic vacancy]. Spinels present in the oxide mixtures were cubic except for Cu4MnAl calcines obtained at 600, 700, and 800 °C, where the mean Mn valence was very close to 3. A similar tetragonal spinel with $a = 8.209$ Å and $c = 8.280$ Å is included in the PDF database ($CuMnAlO_4$, card 43-285 [11]). We used another choice of tetragonal cell, I41/amd; considering this formal difference the lattice parameters are, however, in reasonable agreement. The lattice parameters of several stoichiometric $CuMn_2O_4$ cubic spinels that can be found in the PDF database [11] vary between 8.30 Å and 8.37 Å. If the ratio of Cu and Mn is increased above 1:2, *a* is around 8.30 Å according to the data given in the PDF2 database. Replacing a part of Mn by Mg does not have a great influence on the spinel lattice parameter: $CuMg_{0.5}Mn_{1.5}O_4$ with a disordered cationic occupation in octahedral sites (card 32-343 [11]) has $a = 8.316$ Å. The lattice parameters of the spinels in calcines Cu4Mn2 and Cu2Mg2Mn2 varied in similar ranges. Because

Table 4 The results of XRD data processing of Cu4MnAl calcines. Abbreviations as in Table 2. The 300 °C and 400 °C calcines contained nanocrystalline periclase with (d≈2.45 and 2.10 Å). All crystalline species are included. Approximate spinel formula is $Cu_{0.9}Mn_{1.1}Al_{1.0}O_4$

Parameter	400 °C	500 °C	600 °C	700 °C	800 °C
Tenorite content (%)[a]	–	71	57	57	59
Tenorite integral intensity (arbitrary units)[b]	50	249	348	459	544
Tenorite$D$ (nm)	–	7	11	16	44
Spinel integral intensity (arbitrary units)	–	7[c]	40[d]	51[d]	73[d]
Spinel$a$ (Å)	–	8.214(8)[e]	5.857(3)	5.859(2)	5.850(1)
Spinel$c$ (Å)	–	–	8.141(9)	8.133(5)	8.168(2)
Spinel pseudocubic lattice parameter $a' = \sqrt{[3]}2a^2c$ (Å)	–	–	8.218	8.217	8.221
Spinel$D$ (nm)	–	5	10	15	35
R_{WP}	–	–	15.2	16.6	18.6

[a]Percentage in crystalline fraction
[b]Sum of diffraction lines (200) and (111)
[c]Diffraction line (400)
[d]Sum of diffraction lines (004) and (220)
[e]Fitted as a cubic spinel because of its low crystallinity

Table 5 The results of XRD data processing of Cu2Mg2MnAl calcines. Abbreviations as in Table 2. The 300, 400, and 500 °C calcines contained only nanocrystalline periclase with d≈2.45 and 2.10 Å. All crystalline species are included. Approximate spinel formula is $Cu_{0.5}Mg_{1.2}Mn_{0.7}Al_{0.7}O_4$

Parameter	600 °C	700 °C	800 °C
Tenorite content (%)[a]	26	31	33
Tenorite integral intensity (arbitrary units)[b]	114	242	387
Tenorite$D$ (nm)	5	11	27
Spinel integral intensity (arbitrary units)[c]	102	156	140
Spinel$a$ (Å)	8.265(3)	8.263(2)	8.245(1)
Spinel$D$ (nm)	10	15	46
R_{WP}	16.1	16.4	17.3

[a]Percentage in crystalline fraction
[b]Sum of diffraction lines (200) and (111)
[c]Diffraction line (400)

Al^{3+} has a smaller diameter than Mn^{3+}, spinels in Al-containing calcines have smaller a (Table 5); in Table 4 a pseudocubic lattice parameter a' can be used for the comparison with a of cubic spinels.

Tenorite is known to accommodate only a very small degree of isomorphous substitution [15], with a possible exception of few at% at very low calcination temperatures (350 °C, [16]). On the other hand, spinels can contain any elemental constituent present in the system, with the actual stoichiometry of the cations "adjusted" by Mn valence and the possible presence of cationic vacancies. To perform quantitative XRD analysis, the patterns were hence processed in the following manner: the phase composition was fitted using pure tenorite and an initial model of spinel oxide, e.g. $CuMn_2O_4$ in the Cu4Mn2 calcines. From the resulting percentage of tenorite, the corresponding spinel elemental composition was recalculated, taking into account the total elemental composition from chemical analysis. The mean Mn formal valence obtained by chemical analysis was always larger than the mean valence calculated assuming M_3O_4 spinel stoichiometry, so the difference was corrected by introducing a corresponding percentage of vacancies ($M_{3(1-x)}O_4$, $0 < x < 0.05$) distributed uniformly in tetrahedral and octahedral cationic sites. The new estimate of the spinel composition was used to improve the initial model for the XRD fitting that yields new estimates of the percentage of the components, and the procedure was repeated until a satisfactory agreement was achieved between elemental and phase composition. The occupation of tetrahedral and octahedral sites in the spinel lattice was refined to obtain the best fitting of the intensities of the first two spinel diffraction lines (111) and (220) that are most markedly dependent on the distribution of heavier and lighter metal ions in those sites. This step of the refinement was controlled by minimizing R_{WP}. The cationic distribution was refined only to obtain the best estimate of the percentages of the components and it is not reported here. The correctness of this procedure was checked in the case of Cu4Mn2 calcines. According to XRD fitting and the total Cu and Mn available in the calcines, the Cu/Mn ratio in spinel grew from 0.45/0.55 at 400 °C to 0.40/0.60 at 800 °C, with a correspondingly increasing content of free tenorite. The lattice parameters of the spinels agreed satisfactorily with $a = 8.305$ Å reported for $Cu_{1.4}Mn_{1.6}O_4$ (JCPDS card 35-1030 [11]) and $a = 8.336$ Å reported for $Cu_{1.2}Mn_{1.8}O_4$ (JCPDS card 35-1029 [11]).

The poorly crystalline components of the calcines obtained at 300–500°C were found directly according to

the position of one or two wide diffraction lines (FWHM about 3° in the 2θscale). A single diffraction line at $d \approx 2.4$ Å in the Cu4Mn2 calcines was attributed to a highly disordered phase. The couple of diffraction lines at $d \approx 2.4$ and 2.1 Å, also reported to occur in 500 °C calcines of Ni,Mn [9] and Ni,Mg,Al precursors [14], resembled the pattern of rock-salt-like periclase (MgO). The periclase intermediate was found to be formed as a primary dehydration/decarbonation product of Ni,Al hydrotalcite and assumed to bound both these cations [3], although Al^{III} does not form thermodynamically stable periclase structures. However, it was not possible to use this structural model for a XRD full-profile fitting of this species owing to the disagreement of diffraction line intensities, and hence the quantitative analysis of XRD patterns only counted with the well-crystalline portion of the sample. In addition to the full-profile fitting of the crystalline part of the samples, we calculated integral intensities of two tenorite, (200) and (111), and one spinel, (400), diffraction lines, which were sufficiently intense and did not suffer overlaps with other crystalline or amorphous components. Both integral intensities and the results of the full-profile XRD pattern fitting are summarized in Tables 2, 3, 4, 5. Obviously there was an amorphous portion present in the calcines at least up to 700 °C in all series studied. For example, in the Cu4Mn2 series the tenorite to spinel ratio in the crystalline portion was almost constant between 400 and 700 °C, but the integral diffraction intensities of the individual crystalline components increased considerably (Table 2), demonstrating the crystallization of the amorphous XRD-invisible portion of low-temperature calcines. The integral intensities of the crystalline phases converged to a constant value at 700 °C in the absence of Al, and at even higher temperatures in the presence of Al.

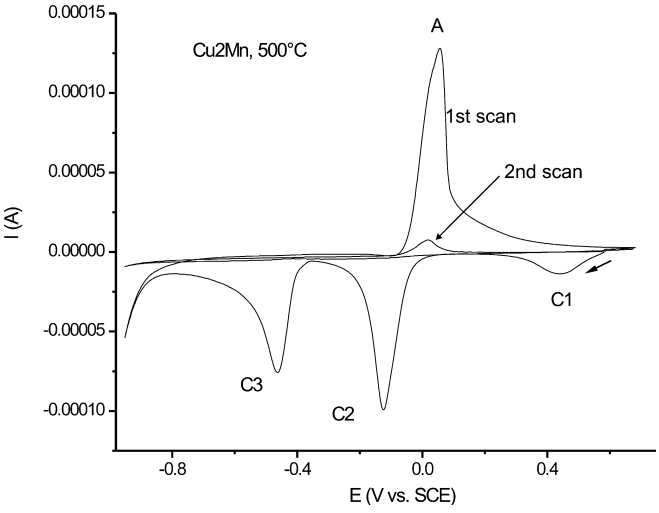

Fig. 1 Designation of peaks in the cyclic voltammetric curves of calcines obtained at 500 °C

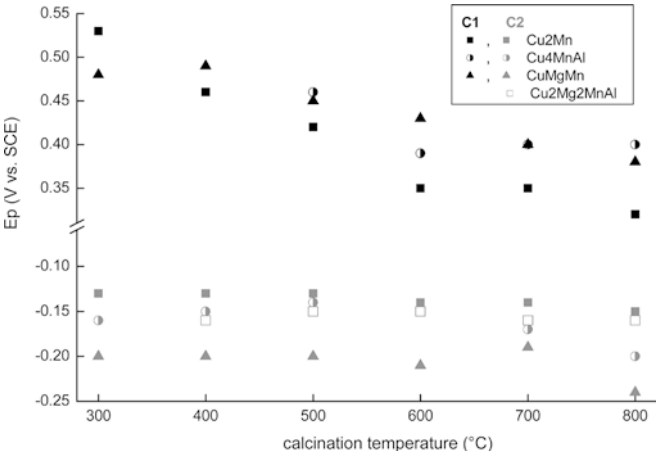

Fig. 2 The dependence of the potentials of peaks C1 and C2 on the calcination temperature

VMP peak identification

Voltammograms of the oxide mixtures (Figs. 1 and 2) had three cathodic (C1 to C3) and one anodic (A) peaks. C1 was present in samples containing spinels with Mn^{IV}, especially in Cu4Mn2, but also in Mg4Mn2. C1 had no anodic counterpart, i.e. the process is chemically irreversible. The potential of C1 was pH dependent with a slope of about −100 mV per pH unit, and also depended on the calcination temperature (Fig. 2). In individual calcines at a given temperature, the peak C1 is more positive in samples with a higher Mn formal valence. C1 occurred at the potential typical for reductive dissolution of MnO_2 and other Mn^{IV}-containing oxides [12]. However, while MnO_2 is completely dissolved at the potential of C1, peak C1 of Cu,Mn and Mg,Mn spinels was always followed by a further cathodic peak C2, which means that some solid-to-solid transformation involving e^- and H^+ is responsible for C1 in the latter case. Assuming the occurrence of copper in the non-stoichiometric spinel oxide as Cu^{II} and manganese as Mn^{III} and Mn^{IV}, the process responsible for C1 could be simplified by the following equation:

$$Cu^{II}_{1.3}Mn^{III}Mn^{IV}_{0.6}O_4(s) + xH^+ + xe^- \rightarrow \left[H_xCu^{II}_{1.3}Mn^{III}_{1+x}Mn^{IV}_{0.6-x}O_4\right](s) \quad (2)$$

where $x < 0.6$. Square brackets stand for a hypothetical solid intermediate, (s) for the solid state. The spinel formula used in the left side of Eq. 2 was taken from Table 2. Peak C1 is almost missing in the series Cu2Mg2MnAl, although the formal Mn valence is almost 4 (Table 5), perhaps because Eq. 2 is suppressed by Al substitution.

C2 was a major peak in voltammograms of amorphous solids in low-temperature calcines, but it was also present in all well-crystalline mixed oxides containing $Mn^{III,IV}$ spinels, including the Cu-free Mg4Mn2 series. The potential of C2 corresponds to reductive dissolution of Mn^{III} oxides [13], but reduction of Cu^{2+} from a solution of $CuSO_4$ and solid malachite proceeded at almost the same potential as C2. The potential of C2 was

almost pH independent. If the anodic scanning followed immediately after registering the peak C2, the reoxidation of Cu^0 (peak A) appeared in the reverse scanning in cyclic voltammetry. The process responsible for C2 is hence mainly attributable to spinel dissolution via Mn^{III} reduction to soluble Mn^{2+} ions, accompanied by a partial reduction of Cu^{2+} (Eq. 3) and/or reduction of free Cu^{2+} ions solubilized from salts of Cu^{II} (Eq. 4):

$$\left[H_{0.6}Cu^{III}_{1.3}Mn^{III}_{1.6}O_4\right](s) + 7.4H^+ + (1.6+2x)e^- \rightarrow 4H_2O + (1.3-x)Cu^{2+} + xCu^0(s) + 1.6Mn^{2+} \quad (3)$$

$$Cu^{2+}(aq) + 2e^- \rightarrow Cu^0(s) \quad (4)$$

From the actual value of the charges of peaks C1 and C2, Q_{C1}/Q_{C2}, x in Eq. 3 could be estimated in well-crystalline samples, because the Mn valence is known from chemical analysis and the Cu amount in the spinel can be calculated from the total Cu and Mn content of the elemental analysis and the CuO content of the XRD phase analysis. However, the Q_{C1}/Q_{C2} value only indicated that x was between 0 and 1, within an uncertainty of the charge measurements and voltammogram fitting. Attempts to decrease the error of the charge evaluation failed and the results of cathodic charge distributions were hence evaluated only graphically.

C3 was present in all samples containing tenorite, and also in some samples that were XRD amorphous or nanocrystalline. The peak potential of C3 was almost pH independent, and it was always followed by the anodic peak A (reoxidation of Cu^0). The overpotential of C3 with respect to C2 of Cu^{2+} was as large as 0.3 V. The peak C3 was the only peak present in pure XRD-crystalline tenorite. The presence of C3 hence clearly indicated the presence of tenorite:

$$CuO(s) + H_2O + 2e^- \rightarrow Cu^0(s) + 2OH^- \quad (5)$$

Thermal crystallization of oxide mixtures

Because of the uncertainty of x in Eqs. 3 and 4, the ratios of the charges of peaks C1, C2, C3, and A were interpreted as fingerprints of the components and the phase composition of the samples was inferred from the temperature dependences of the charge ratios. Q_{C1}/Q_{C3} is proportional to the ratio of spinel to tenorite, while the growth of Q_{C1}/Q_{Ctot} and Q_{C3}/Q_{Ctot} ($Q_{Ctot} = Q_{C1} + Q_{C2} + Q_{C3}$) indicates the crystallization of spinel and tenorite from the primary hydrotalcite decomposition products. The crystallization course of Cu4Mn2 and Cu2Mg2Mn2 samples according to voltammetry is shown in Fig. 3, where the contributions of C1, C2, and C3 to the total cathodic charge Q_{Ctot} are compared at changing calcination temperatures. In Fig. 4, Q_{C1}/Q_{C3} dependence on the calcination temperature is plotted against the calcination temperature for the Cu4Mn2 and Cu2Mg2Mn2 series. The difference between the two series is obvious.

Cu4Mn2 crystallization was practically finished at 400 °C according to VMP but at 700 °C according to XRD (Table 2, integral intensities of crystalline components), and the ratio of spinel and tenorite was almost constant in the temperature range 300–700 °C according

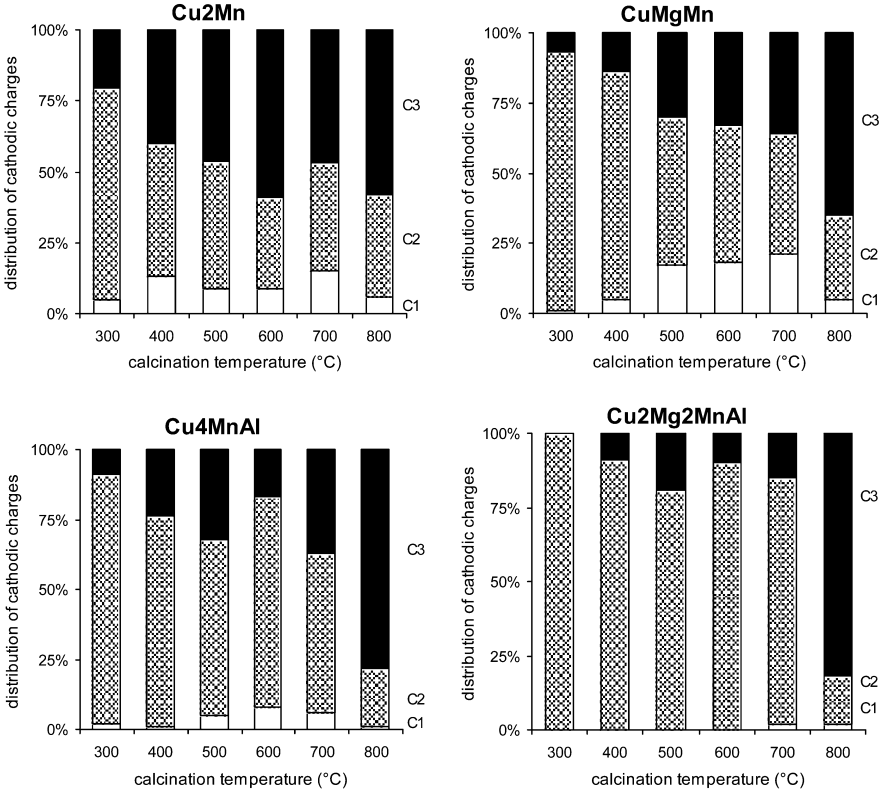

Fig. 3 The distribution of cathodic charges between the peaks C1, C2, and C3

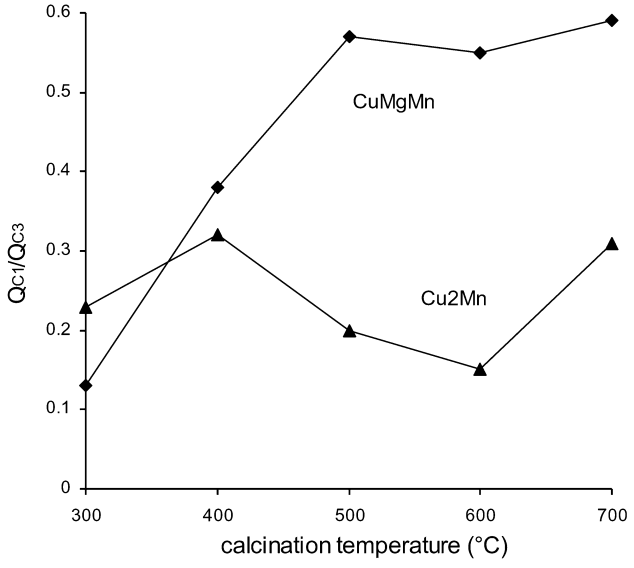

Fig. 4 The dependence of the charge ratio Q_{C1}/Q_{C3} in the series Cu4Mn2 and Cu2Mg2Mn2

to both methods. The particle sizes obtained from XRD line-broadening grew significantly in this temperature range. All observations hence indicated that the amorphous matter had the same chemical composition as the crystalline products, and that crystallization of the precursors at >300 °C proceeded smoothly without any additional crystalline intermediate, with formation of nanocrystalline products being finished at about 400 °C according to VMP; charge distribution (Fig. 3, Cu4Mn2) was almost constant above 400 °C.

In the Cu2Mg2Mn2 series, tenorite and spinel formation was finished at 500 °C according to VMP, and between 300 and 500 °C the spinel to tenorite ratio increased. XRD confirmed this sequence of crystallization by both analysis of the crystalline portion and by the thermal dependence of the integral intensities of tenorite and spinel (Table 3). The primary crystallization of tenorite before spinel can be explained by two hypotheses: either CuO nuclei had already been present in the precursor, or CuO was formed first, leaving a Cu-depleted intermediate. The latter explanation is confirmed by the presence of the nanocrystalline periclase intermediate that could certainly bind the majority of Mg and possibly also the Mn necessary to form later the spinel lattice; this periclase intermediate was missing in Cu4Mn2. This explanation stresses the importance of the precursor structure for crystallization of the Cu,Mn oxides. The periclase intermediate is formed from the brucite octahedral layers of the hydrotalcite by its shrinking along the *c*-axis owing to removal of the interlayer carbonates; the shrunken octahedral layers then yield the (111) crystal plane of periclase. This reaction mechanism is in line with the preferential formation of the (111) crystal plane of the periclase-derived murdochite phase Ni_6MnO_8 on the decomposition of Ni2Mn hydrotalcite [17]. The periclase intermediate cannot be expected in the Cu4Mn2 precursor, first of all because it did not have the hydrotalcite structure, and also because no periclase-promoting metal ions are available in the Cu4Mn2 system.

In the Al-containing series, peak C1 was suppressed, and especially in the Cu2Mg2MnAl series it was practically absent. This fact can have two reasons: either Al substitution in the spinel suppressed the spinel reactivity, similar to Al or Cr substitution in Fe oxides [18], or the spinel formation was inhibited by the Al presence. The presence of Al in the spinel was proven by its smaller lattice parameters (Tables 2, 3, 4, 5), owing to the smaller ionic radius of Al^{III} with respect to Cu^{II}, Mg^{II}, Mn^{III}, and Mn^{IV}. In both Al-containing series calcined up to 700 °C, C2 was the dominant cathodic peak, indicating a major portion of amorphous intermediates, and only at 800 °C did $Q_{C3} > Q_{C2}$ prove the dominance of CuO over spinel. The slowed-down crystallization of oxide mixtures by Al^{III} was also proven by the continuous increase of the integral intensities of the CuO and spinel XRD lines (Tables 4 and 5). XRD lines of tenorite and spinels appeared as late as at 600 °C and further grew at 700 and 800 °C. The presence of XRD-amorphous matter in Al-containing hydrotalcite calcines surviving relatively high calcination temperatures is a well-known phenomenon [14]. However, VMP clearly indicated the presence of CuO in Al-containing calcines obtained at 400 °C. Obviously, CuO formation was not suppressed, but its mean coherence length was too small to be detected by XRD.

Conclusion

VMP indicated the presence of the crystallization products tenorite and spinel in calcines obtained at temperatures of 400 and 500 °C. The crystallization of mixed oxides, which were formed during thermal treatment of a Cu- and Mn-containing precursor according to both VMP and XRD, can be summarized by the following schemes of crystallization of the individual oxide services:

$$\text{Cu4Mn2 precursor} \xrightarrow{300\,^\circ\text{C}} \text{amorphous} + \text{tenorite} + \text{Mn}^{\text{IV}}\ \text{spinel} \xrightarrow{400\,^\circ\text{C}} \text{tenorite} + \text{Mn}^{\text{IV}}\ \text{spinel} \xrightarrow{500-700\,^\circ\text{C}} \text{growth of tenorite and spinel particles} \quad (6)$$

$$\text{Cu2Mg2Mn2 hydrotalcite} \xrightarrow{300\,^\circ\text{C}} \text{nanocrystalline periclase} + \text{tenorite} \xrightarrow{400\,^\circ\text{C}} \text{amorphous} + \text{tenorite} + \text{Mn}^{\text{IV}}\ \text{spinel} \xrightarrow{500\,^\circ\text{C}} \text{tenorite} + \text{Mn}^{\text{IV}}\ \text{spinel} \xrightarrow{600-800\,^\circ\text{C}} \text{growth of spinel and tenorite particles} \quad (7)$$

In the crystallization schemes, the term amorphous stands for XRD-amorphous components (indicated indirectly by low integral intensities of the diffraction lines of crystalline components); that species is responsible for the voltammetric peak C2. Further growth of calcination temperatures above 400 °C (Cu4Mn2) and 500 °C (Cu2Mg2Mn2) only caused growth of the tenorite and spinel particle sizes.

In Al-containing Cu,Mn oxides, the crystallization shifted to higher temperatures, with tenorite being formed before spinel:

Cu4MnAl hydrotalcite

$$\xrightarrow{300\,^{\circ}C} \text{nanocrystalline periclase} + \text{nanocrystalline tenorite}$$

$$\xrightarrow{400\,^{\circ}C} \text{nanocrystalline periclase} + \text{tenorite}$$

$$\xrightarrow{500\,^{\circ}C} \text{amorphous} + \text{tenorite} + \text{Mn}^{\text{IV}}\ \text{spinel}$$

$$\xrightarrow{600-800\,^{\circ}C} \text{growth of tenorite and spinel particles} \qquad (8)$$

Cu2Mg2MnAl hydrotalcite

$$\xrightarrow{300\,^{\circ}C} \text{nanocrystalline periclase}$$

$$\xrightarrow{400\,^{\circ}C,500\,^{\circ}C} \text{nanocrystalline periclase} + \text{tenorite}$$

$$\xrightarrow{600\,^{\circ}C} \text{amorphous} + \text{tenorite} + \text{spinel}$$

$$\xrightarrow{700-800\,^{\circ}C} \text{growth of tenorite and spinel particles} \qquad (9)$$

The structure binding the residual carbonates in Cu-containing samples evolved at 480–600°C remains unclear.

Acknowledgements The work was supported by grants CEZ:MSM 223/10/0002 and LN00A028 funded by the Ministry of Education, Youth and Sports of the Czech Republic.

References

1. Wright PA, Natarajan S, Thomas JM (1992) Chem Mater 4:1053
2. Bellotto M, Rebours B, Clause O, Lynch J, Bazin D, Elkaim E (1996) J Phys Chem 100:8527
3. Bellotto M, Rebours B, Clause O, Lynch J, Bazin D, Elkaim E (1996) J Phys Chem 100:8535
4. Jirátová K, Čuba P, Kovanda F, Hilaire L, Pitchon V (2002) Catal Today 76:43
5. Wöllner A, Lange F, Schmelz H, Knözinger H (1993) Appl Clay Sci 94:181
6. Doménech A, Pérez-Ramírez J, Ribera A, Mul G, Kapteijn F, Arends IWCE (2002) J Electroanal Chem 519:72
7. Grygar T, Bezdička P, Hradil D, Pikna L (2003) Solid State Phenom 90/91:45
8. Kovanda F, Jirátová K, Rymeš J, Koloušek D (2001) Appl Clay Sci 18:71
9. Barriga C, Fernández JM, Ulibarri MA, Labajos FM, Rives V (1996) J Solid State Chem 124:205
10. ICSD database (2002) FIZ Karlsruhe, Germany, release 2002/1
11. JCPDS PDF-2 database (2002) International Center for Diffraction Data, Newtown Square, Pa., USA, release 52
12. Bakardjieva S, Bezdička P, Grygar T, Vorm P (2000) J Solid State Electrochem 4:306
13. Grygar T, Bakardjieva S, Bezdička P, Vorm P (2001) Ceram Silikáty 45:55
14. Rives V, Kannan S (2000) J Mater Chem 10:489
15. Grygar T, Salátová Z, Vorm P (2001) Ceram Silikáty 45:121
16. Ketchik SV, Minyukova TP, Kuznetsova LI, Plyasova LM, Yurieva TM, Boreskov GK (1982) React Kinet Catal Lett 19:345
17. Kovanda F, Grygar T, Dorničák V (2003) Solid State Sci 5:1019
18. Grygar T (1997) J Solid State Electrochem 1:77